

This discussion paper is/has been under review for the journal *Climate of the Past* (CP).
Please refer to the corresponding final paper in CP if available.

Natural variability and anthropogenic effects in a Central Mediterranean core

S. Alessio¹, G. Vivaldo¹, C. Taricco¹, and M. Ghil^{2,3}

¹Dipartimento di Fisica Generale dell'Università, and Istituto di Fisica dello Spazio Interplanetario (IFSI-INAf), Torino, Italy

²Geosciences Department & Laboratoire de Météorologie Dynamique (CNRS and IPSL), Ecole Normale Supérieure, Paris, France, and Department of Atmospheric and Oceanic Sciences & Institute of Geophysics and Planetary Physics, University of California, Los Angeles, CA 90095-1565, USA

³Department of Atmospheric and Oceanic Sciences & Institute of Geophysics and Planetary Physics, University of California, Los Angeles, CA 90095-1565, USA

Received: 17 September 2011 – Accepted: 9 October 2011 – Published: 27 October 2011

Correspondence to: C. Taricco (carla.taricco@unito.it)

Published by Copernicus Publications on behalf of the European Geosciences Union.

Natural variability and anthropogenic effects in a Central Mediterranean core

S. Alessio et al.

Title Page

Abstract

Introduction

Conclusions

References

Tables

Figures

⏪

⏩

◀

▶

Back

Close

Full Screen / Esc

Printer-friendly Version

Interactive Discussion

Abstract

We evaluate the contribution of natural variability to the modern decrease in foraminiferal $\delta^{18}\text{O}$ by relying on a 2200-years-long, high-resolution record of oxygen isotopic ratio from a Central Mediterranean sediment core. Pre-industrial values are used to train and test two sets of algorithms that are able to forecast the natural variability in $\delta^{18}\text{O}$ over the last 150 yr. These algorithms are based on autoregressive models and neural networks, respectively; they are applied separately to each of the $\delta^{18}\text{O}$ series' significant variability components, rather than to the complete series. The separate components are extracted by singular-spectrum analysis and have narrow-band spectral content, which reduces the forecast error. By comparing the sum of the predicted components to the actual values during the Industrial Era, we deduce that the natural contribution to the modern $\delta^{18}\text{O}$ variation decreased gradually, until it reached roughly 40 % as early as the end of the 1970s.

1 Introduction

In a previous paper (Taricco et al., 2009), we presented a high-resolution record of foraminiferal $\delta^{18}\text{O}$ isotopic ratio that covers the last two millennia. This record was obtained from a shallow-water sediment core drilled in the Central Mediterranean (Galipoli Terrace in the Gulf of Taranto, Ionian Sea) and was dated with high accuracy by tephroanalysis and radiometric measurements. The $\delta^{18}\text{O}$ series so obtained spans the last 2200 years and was analyzed by singular-spectrum analysis (SSA; see Vautard and Ghil, 1989; Ghil and Vautard, 1991; Plaut et al., 1995; Ghil and Taricco, 1997; Ghil et al., 2002 and references therein). This analysis revealed highly significant decadal, centennial and multicentennial oscillatory components, along with a millennial trend.

The $\delta^{18}\text{O}$ profile shows a steep decrease during the Industrial Era; see gray light curve in Fig. 1. In this paper, we address the problem of evaluating the contribution of natural climate oscillations to this modern variation: pre-industrial $\delta^{18}\text{O}$ variations are

CPD

7, 3699–3718, 2011

Natural variability and anthropogenic effects in a Central Mediterranean core

S. Alessio et al.

Title Page

Abstract

Introduction

Conclusions

References

Tables

Figures

⏪

⏩

◀

▶

Back

Close

Full Screen / Esc

Printer-friendly Version

Interactive Discussion



used to design and tune algorithms able to forecast the natural variability in the $\delta^{18}\text{O}$ series over the last 150 yr. The comparison between the forecast and the actual $\delta^{18}\text{O}$ signal during the Industrial Era allows one to quantify what percentage of the modern $\delta^{18}\text{O}$ decrease can be attributed to natural vs. anthropogenic causes.

Two independent methods of time series prediction are considered here: (i) autoregressive (AR) models (Box and Jenkins, 1970; Childers, 1978; Montgomery et al., 1990); and (ii) feed-forward neural networks (Hagan et al., 1996; Haykin et al., 1999). Since all prediction methods work better on clean, noise-free signals, the predictions here are not performed directly on the $\delta^{18}\text{O}$ series, but rather on each significant variability component extracted by SSA, as suggested by Penland et al. (1991), Keppenne and Ghil (1992, 1993) and Ghil et al. (2002). The $\delta^{18}\text{O}$ forecast is then obtained by summing the contributions of all components.

The paper is organized as follows. In the next section we present briefly the record and its statistically significant oscillatory components. The prediction methodology is introduced in Sect. 3, while the results and their discussion follow in Sect. 4. Section 5 presents the conclusions.

2 The $\delta^{18}\text{O}$ record and its spectral analysis

The marine sediment core GT90/3 we use here was extracted from the Gulf of Taranto, Ionian Sea (39°45'53" N, 17°53'33" E), at a depth of about 200 m, and is 3.57 m-long. Several papers (Bonino et al., 1993; Cini Castagnoli et al., 1990, 1992a,b, 1997, 1998, 1999, 2002a,b, 2005; Taricco et al., 2008; Vivaldo et al., 2009) described the dating of the core and previous measurements in the shells of the foraminiferal species *Globigerinoides ruber* performed in samples from it; these measurements covered the last millennium. Taricco et al. (2009) extended the measurements of the $\delta^{18}\text{O}$ isotopic ratio down-core, to cover the last 2200 yr.

The $\delta^{18}\text{O}$ time series spans 188 BC–1979 AD and it consists of 560 samples with a sampling interval of $\Delta t = 3.87$ yr; the raw data set is shown in Fig. 1 (gray light curve).

Natural variability and anthropogenic effects in a Central Mediterranean core

S. Alessio et al.

Title Page

Abstract

Introduction

Conclusions

References

Tables

Figures

⏪

⏩

◀

▶

Back

Close

Full Screen / Esc

Printer-friendly Version

Interactive Discussion



Natural variability and anthropogenic effects in a Central Mediterranean core

S. Alessio et al.

Title Page

Abstract

Introduction

Conclusions

References

Tables

Figures

⏪

⏩

◀

▶

Back

Close

Full Screen / Esc

Printer-friendly Version

Interactive Discussion



The SSA of this series revealed highly significant oscillatory components of roughly 600 yr, 350 yr, 200 yr, 125 yr and 11 yr (Taricco et al., 2009). These oscillations were captured, respectively, by reconstructed components (RCs) 2–3, 4–5, 6–7–8, 9–10 and 11–12; a millennial trend, captured by RC 1, is present as well. In this paper, we are interested in centennial-to-millennial variability and therefore we neglect the decadal component (RCs 11–12). The total SSA reconstruction of the low-frequency variability (LFV) of interest here, y_{obs} , is given by:

$$y_{\text{obs}} = \text{RCs}_{1-10} + \bar{y}, \quad (1)$$

where \bar{y} indicates the mean value of the raw $\delta^{18}\text{O}$ data; y_{obs} is shown as the black heavy curve in Fig. 1. The trend alone is plotted in Fig. 1 as the red heavy curve, while the individual oscillatory components are shown in Fig. 2.

3 Prediction methodology

Our approach in the present work is based on two reasonable assumptions:

- before 1840 AD the influence of human activities on climate, and therefore on $\delta^{18}\text{O}$ values, was negligible; and
- $\delta^{18}\text{O}$ values from the early-to-mid 19th century on contain both natural and anthropogenic signals.

Thus the long pre-1840 section of the series, representing natural $\delta^{18}\text{O}$ variability, with $N = 524$ samples, is employed to first fit and then test the performance of our two prediction methods, based respectively on: (i) AR models, and (ii) neural networks. The prediction is next performed on the 1840–1979 AD interval, comprising $L_{\text{max}} = 36$ samples. As illustrated in Fig. 3, the series is thus divided into three sections: learning, testing, and forecasting. Recall that the sampling interval is $\Delta t = 3.87 \text{ yr} \approx 4 \text{ yr}$ and so, for instance, $L_{\text{max}} \Delta t \approx 140 \text{ yr} = 1979 - 1840 \text{ yr}$.

(i) SSA-AR prediction

To be precise, the first method is a combined SSA-AR method, as introduced by Kepenne and Ghil (1992, 1993) and further described in Ghil et al. (2002); it is implemented in the toolkit available at <http://www.spectraworks.com/web/products.html>.

The basic idea is that the RCs in SSA are data-adaptively filtered signals, each of which is dominated by a narrow spectral peak (Penland et al., 1991). Such narrow-band signals allow much more accurate predictions than broad-band ones.

We chose to predict separately each of five narrow-band signals contained in our time series, namely the four oscillatory ones shown in Fig. 2 and the trend shown as the red heavy curve in Fig. 1. The five predictions of RCs 1, 2–3, 4–5, 6–8 and 9–10 are then summed to yield the total prediction y_{pred} .

The SSA-AR method turns out to be most reliable and robust when the order M_{AR} of the autoregressive model fitted to the data is similar to the SSA embedding dimension M_{SSA} , $M_{\text{AR}} \approx M_{\text{SSA}}$. This result follows from the way the SSA lag-covariance matrix and the Burg algorithm's AR coefficients are computed in the combined SSA-AR algorithm.

Moreover, it is good practice to use an order M_{AR} that, like the SSA embedding dimension M_{SSA} , is not too large with respect to the length N of the time series, since the variance of the AR-coefficient estimates increases with the order. As recommended by Vautard et al. (1992), we use a section of length $N_{\text{learn}} = 3M_{\text{SSA}}$ for the learning, with $M_{\text{SSA}} = 60$.

Since the actual prediction is performed with a maximum lead of $L_{\text{max}} = 36$, we first evaluate the prediction skill by cross-validating over the test section with the same maximum lead.

Our testing approach is aimed at assessing the forecast skill as a function of lead time, in terms of the root-mean-square (rms) error between predicted and true values, which should be as small as possible, as well as the correlation between forecast and true values, which should be as large as possible. We thus need to verify in the

Natural variability and anthropogenic effects in a Central Mediterranean core

S. Alessio et al.

Title Page

Abstract

Introduction

Conclusions

References

Tables

Figures

⏪

⏩

◀

▶

Back

Close

Full Screen / Esc

Printer-friendly Version

Interactive Discussion



test section several predictions with L steps ahead, up to and including L_{\max} . This is achieved by carrying out the iterative scheme shown in Fig. 3a1.

In this approach, the length of the test section is $N_{\text{test}} = N - 3M_{\text{SSA}} = 344$ samples. A sliding window of fixed length $K = N - 3M_{\text{SSA}} - L_{\max} = 308$ samples shifts ahead, depending on the lead time considered for testing, as illustrated by the red segments in Fig. 3a1. For a value L of the lead, we thus set the initial and final points of the sliding window at $x_i = 3M_{\text{SSA}} + L$ and $x_f = 3M_{\text{SSA}} + L + K$, respectively. For instance, when $L = 1$, the sliding window that provides the K pairs of predicted–true values for skill assessment starts at the sample $x_i = 3M_{\text{SSA}} + 1 = 181$ and ends at the sample $x_f = 3M_{\text{SSA}} + K + 1 = 489$ while, when $L = L_{\max}$, the sliding window starts at the sample $x_i = 3M_{\text{SSA}} + L_{\max} = 216$ and ends at $x_f = N = 524$, which is the last sample (1840 AD).

For any position of the sliding window, corresponding to a lead time L , each one of the K samples that form the window is predicted using M true values as inputs: samples from $x(n+1-M)$ to $x(n)$ are used to forecast $x(n+L)$, by applying an iterative, one-step-into-the-future procedure, according to the equations

$$x(n+1) = a_1 x(n) + a_2 x(n-1) + \dots + a_M x(n+1-M), \quad (2)$$

$$x(n+2) = a_1 x(n+1) + a_2 x(n) + \dots + a_M x(n+2-M),$$

.....

$$x(n+L) = a_1 x(n+L-1) + a_2 x(n+L-2) + \dots + a_M x(n+L-M).$$

In system Eq. (2), we have dropped the subscript AR from M_{AR} for simplicity, and will do so below. When predicting the first sample of the sliding window in its L -th position, only samples out of the learning section are used as inputs, but moving toward the K -th and last window sample, more and more true values from the test section are employed. The rms error $R = R(L)$ thus evaluated quantifies the prediction skill at the particular lead time L . An example of this procedure, for the case $L = 10$, is shown in Fig. 3a2.

Natural variability and anthropogenic effects in a Central Mediterranean core

S. Alessio et al.

Title Page

Abstract

Introduction

Conclusions

References

Tables

Figures



Back

Close

Full Screen / Esc

Printer-friendly Version

Interactive Discussion



signals. This approach allowed us to choose the network architecture that best reproduces the samples in the test section, which has fixed length N_{test} , as in Fig. 3b.

For this purpose, a Matlab code was written, employing the functions of its Neural Network Toolbox. The training was performed using the Levenberg-Marquardt algorithm (Rumelhart, 1986; Hagan and Menhaj, 1994). This algorithm is best suited for the type of problem at hand, in which the net is small or of medium size – with less than one hundred weights, say – and the approximation must therefore be very accurate.

The trained network is used to forecast the $\delta^{18}\text{O}$ -values in the test section, using an iterative, one-step-into-the-future procedure, as done for the SSA-AR prediction. The last l elements of the learning section are used to predict the first sample of the test section. Then the first predicted sample of the test section is inserted into the next input vector to get the second forecast, and so on, until the 64-steps-into-the-future forecast is produced and the end of the test section is attained; see again Fig. 3b.

The best-performing net is chosen, i.e. the one that has the smallest global rms error over the entire test section. This optimal net is then used for calculating the 36 samples of the post-1840 forecast, which are produced in the same way as the test-section forecasts.

The dependence of the training process of each net on the random choice of the initial guesses for weights and biases suggested running the program a number of times for each narrow-band signal and then averaging the forecasts over all the runs. Finally, the average forecasts for the five narrow-band signals were summed to yield the total average prediction y_{pred} .

The 36 predicted values $\{y_{\text{pred}}(j) : j = 1, \dots, 36\}$ of $\delta^{18}\text{O}$ for the interval 1840–1979 AD are thus determined, either (i) by an $\text{AR}(M)$ model with order M or (ii) by neural networks. These values represent the natural LFV of the $\delta^{18}\text{O}$ record and are then compared with the values y_{obs} observed after 1840; the latter represent the total variability, natural plus anthropogenic, for the Industrial Era, see Sect. 4 below.

Natural variability and anthropogenic effects in a Central Mediterranean core

S. Alessio et al.

Title Page

Abstract

Introduction

Conclusions

References

Tables

Figures

⏪

⏩

◀

▶

Back

Close

Full Screen / Esc

Printer-friendly Version

Interactive Discussion



Recall that, in fact, the observations y_{obs} have also been low-pass filtered, see Eq. (1). Hence our comparison of natural and anthropogenic variability eliminates higher-frequency contributions, such as year-to-year or, more precisely, sample-to-sample fluctuations.

4 Results and discussion

Figure 4 displays the forecasts obtained by the SSA-AR method (red curves), together with the upper and lower error bounds (pink shading); these error bounds were obtained as explained in the previous section. Panels a–e in the figure show the forecast of the five narrow-band signals that compose our $\delta^{18}\text{O}$ record, while Fig. 4f shows their sum y_{pred} . The black heavy curves in all panels represent observed values. In particular, the one in Fig. 4f corresponds to the one shown in Fig. 1, i.e. y_{obs} , but limited now to the interval $\approx 1740\text{--}1979$ AD.

Figure 5 compares the total AR forecast over the Industrial Era (1840–1979 AD; red curve), accompanied by its error bounds (pink shading), with the low-pass filtered observed $\delta^{18}\text{O}$, namely y_{obs} (black curve), put now into the perspective of the entire 2200-year record. In this figure, we show also the forecast obtained by the neural-network methodology (blue curve). The latter prediction stays within the error bounds of the SSA-AR forecast.

We notice, in particular, that the natural-variability forecast y_{pred} , whether obtained by the AR or neural-network approach, reaches $\delta^{18}\text{O}$ values within the Industrial Era that are as low as those that characterized the Medieval Optimum. The observed values y_{obs} , though, greatly exceed these values, even though our record stops in 1979.

In order to measure the difference between the observed values y_{obs} during the last 150 yr or so and the forecast ones y_{pred} by either prediction method, we define the fraction $V_{\text{nat}}(t)$ of natural variability by

Natural variability and anthropogenic effects in a Central Mediterranean core

S. Alessio et al.

Title Page

Abstract

Introduction

Conclusions

References

Tables

Figures

⏪

⏩

◀

▶

Back

Close

Full Screen / Esc

Printer-friendly Version

Interactive Discussion



$$V_{\text{nat}}(t) = \frac{[y_{\text{pred}}(t) - \mu]^2}{[y_{\text{pred}}(t) - \mu]^2 + [y_{\text{obs}}(t) - y_{\text{pred}}(t)]^2}, \quad (3)$$

where μ is the mean computed over the pre-industrial section of the time series, i.e. before 1840 AD. The fraction $V_{\text{nat}}(t)$ is shown for the AR forecast in Fig. 6 (red curve); the pink shading indicates the range of uncertainty for this fraction, based on the errors in the forecast y_{pred} , using Eq. (3).

In agreement with our assumptions, $V_{\text{nat}}(t)$ equals 100% at the beginning of the Industrial Era (1840 AD in this account), while the anthropogenic contribution remains negligible up to about 1880 AD. Afterwards the natural portion of the LFV decreases gradually to about 40% by the end of the 1970s (top of the core). The blue curve represents the same fraction $V_{\text{nat}}(t)$ calculated from the neural network forecast; the latter does lie within the uncertainty range of the AR estimates, further confirming our confidence in this range.

Comparing the natural $\delta^{18}\text{O}$ variation y_{pred} and the total one y_{obs} in Fig. 4f allows one to draw several conclusions about temperature variation during the last century. As noted by Taricco et al. (2009), the observed modern variation of about $0.5^{\circ}/_{00}$ in $\delta^{18}\text{O}$, if entirely due to temperature effects, would approximately correspond, according to the transfer function of Shackleton and Kennet (1975), to an increase of about 2°C . This estimate is confirmed by alkenone-derived temperature measurements performed in the same sediments by Versteegh et al. (2007).

According to our prediction, the natural variation in $\delta^{18}\text{O}$ over the last century is of about $0.2^{\circ}/_{00}$, which corresponds to 0.8°C . This result suggests that, as early as the end of the 1970s, 60% of the observed temperature increase was already due to anthropogenic effects.

The high increases in temperature values, observed as well as predicted, indicate a local amplification recorded in the core with respect to the modern variation in Northern Hemisphere temperatures. As argued already by Taricco et al. (2009), this amplification is most likely related to the shallow, semi-enclosed nature of the Gulf of Taranto.

Natural variability and anthropogenic effects in a Central Mediterranean core

S. Alessio et al.

Title Page

Abstract

Introduction

Conclusions

References

Tables

Figures

⏪

⏩

◀

▶

Back

Close

Full Screen / Esc

Printer-friendly Version

Interactive Discussion



5 Conclusions

The $\delta^{18}\text{O}$ record in the shallow-water sediment core GT90/3 exhibits a marked modern decrease (Taricco et al., 2009). The remarkable length of this accurately dated $\delta^{18}\text{O}$ series, extending back to 188 BC (Fig. 1), allowed us to separate natural from anthropogenic variability in the modern portion of the record, 1840–1979 AD.

In order to evaluate the contribution of natural variability to the modern $\delta^{18}\text{O}$ decrease, we fitted auto-regressive (AR) models and trained neural networks on the pre-industrial (188 BC–1840 AD) $\delta^{18}\text{O}$ values only. As a noise reduction strategy (Penland et al., 1991), we first applied singular-spectrum analysis (SSA) to extract the statistically significant signals associated with the climate low-frequency variability (LVF); these signals include a millennial trend, captured by reconstructed component (RC) 1 (red curve in Fig. 1), and four oscillatory modes, captured by RCs 2–3, 4–5, 6–8 and 9–10, respectively (Fig. 2). These five narrow-band signals were then fitted and forecast individually, rather than trying to do so for the original, noisy time series.

Both the AR and neural network algorithms were trained and tested on the pre-1840 part of the record, according to the methods outlined schematically in Fig. 3. The post-1840 forecast values of the narrow-band signals (Fig. 4a–e) were then summed (Fig. 4f) and the sum $y_{\text{pred}}(t: 1840 \leq t \leq 1979)$ was assumed to represent the natural variability during the Industrial Era.

The predicted LFV y_{pred} was compared to the total one y_{obs} (Fig. 5), thus allowing us to assess the contribution of natural variability in $\delta^{18}\text{O}$ over the last century-and-a-half. This contribution turned out (Fig. 6) to have decreased steadily from 100 % in the mid-19th century to about 40 % by the end of the 1970s.

Acknowledgements. We wish to thank A. Romero and P. Colombetti for their dedicated technical assistance and S. M. Bernasconi (Geological Institute, ETH, Zürich, Switzerland) for the mass spectrometer measurements of $\delta^{18}\text{O}$. The work of M. G. has been partially supported by NSF grant DMS-1049253.

Natural variability and anthropogenic effects in a Central Mediterranean core

S. Alessio et al.

Title Page

Abstract

Introduction

Conclusions

References

Tables

Figures

⏪

⏩

◀

▶

Back

Close

Full Screen / Esc

Printer-friendly Version

Interactive Discussion



References

- Bonino, G., Cini Castagnoli, G., Callegari, E., and Zhu, G. M.: Radiometric and tephroanalysis dating of recent Ionian sea cores, *Nuovo Cimento C*, 16, 155–161, 1993. 3701
- Box, G. and Jenkins, G.: *Time series analysis: Forecasting and control*, San Francisco, Holden-Day, 1970. 3701
- Childers, D. G.: *Modern Spectrum Analysis*, edited by: Childers, D. G., IEEE Press, New York, 1978 3701
- Cini Castagnoli, G., Bonino, G., Caprioglio, F., Provenzale, A., Serio, M., and Zhu, G. M.: The carbonate profile of two recent Ionian sea cores: evidence that the sedimentation rate is constant over the last millenia, *Geophys. Res. Lett.*, 17, 1937–1940, 1990. 3701
- Cini Castagnoli, G., Bonino, G., Provenzale, A., Serio, M., and Callegari, E.: The CaCO₃ profiles of deep and shallow Mediterranean sea cores as indicators of past solar-terrestrial relationship, *Nuovo Cimento C*, 15, 547–563, 1992a. 3701
- Cini Castagnoli, G., Bonino, G., Serio, M., and Sonett, C. P.: Common spectral features in the 5500-year record of total carbonate in sea sediments and radiocarbon in tree rings, *Radiocarbon*, 34, 798–805, 1992b. 3701
- Cini Castagnoli, G., Bonino, G., Della Monica, P., and Taricco, C.: Record of thermoluminescence in sea sediments in the last millennia, *Nuovo Cimento C*, 20, 1–8, 1997. 3701
- Cini Castagnoli, G., Bonino, G., and Taricco, C.: The global and persistent millennial-scale variability in the thermoluminescence profiles of shallow and deep Mediterranean sea cores, *Nuovo Cimento C*, 21, 453–460, 1998. 3701
- Cini Castagnoli, G., Bonino, G., Della Monica, P., Taricco, C., and Bernasconi, S. M.: Solar activity in the last millennium recorded in the $\delta^{18}\text{O}$ profile of planktonic foraminifera of a shallow water Ionian Sea core, *Solar Phys.*, 188, 191–202, 1999. 3701
- Cini Castagnoli, G., Bonino, G., and Taricco, C.: Long term solar-terrestrial records from sediments: carbon isotopes in planktonic foraminifera during the last millennium, *Adv. Space Res.*, 29, 1537–1549, 2002a. 3701
- Cini Castagnoli, G., Bonino, G., Taricco, C., and Bernasconi, S. M.: Solar radiation variability in the last 1400 years recorded in the carbon isotope ratio of a Mediterranean sea core, *Adv. Space Res.*, 29, 1987–1994, 2002b. 3701

Natural variability and anthropogenic effects in a Central Mediterranean core

S. Alessio et al.

Title Page

Abstract

Introduction

Conclusions

References

Tables

Figures

⏪

⏩

◀

▶

Back

Close

Full Screen / Esc

Printer-friendly Version

Interactive Discussion



Natural variability and anthropogenic effects in a Central Mediterranean core

S. Alessio et al.

Title Page

Abstract

Introduction

Conclusions

References

Tables

Figures

⏪

⏩

◀

▶

Back

Close

Full Screen / Esc

Printer-friendly Version

Interactive Discussion



- Cini Castagnoli, G., Taricco, C., and Alessio, S.: Isotopic record in a marine shallow-water core: imprint of solar centennial cycles in the past 2 millennia, *Adv. Space Res.*, 35, 504–508, 2005. 3701
- 5 Ghil, M. and Taricco, C.: Advanced spectral analysis methods, in: *Past and Present Variability of the Solar-terrestrial System: Measurement, Data Analysis and Theoretical Models*, edited by: Cini Castagnoli, G. and Provenzale, A., IOS Press, Amsterdam, The Netherlands, 137–159, 1997. 3700
- Ghil, M. and Vautard, R.: Interdecadal oscillations and the warming trend in global temperature time series, *Nature*, 350, 324–327, 1991. 3700
- 10 Ghil, M., Allen, M. R., Dettinger, M. D., Ide, K., Kondrashov, D., Mann, M. E., Robertson, A. W., Saunders, A., Tian, Y., Varadi, F., and Yiou, P.: Advanced spectral methods for climatic time series, *Rev. Geophys.*, 40, 3.1–3.41, 2002. 3700, 3701, 3703
- Hagan, M. T. and Menhaj, M. B.: Training feedforward networks with the Marquardt algorithm, *IEEE T. Neural Netw.*, 5, 989–993, 1994. 3706
- 15 Hagan, M. T., Demuth, H. B., and Beale, M. H.: *Neural Network Design*, PWS Publishing, Boston, MA, 1996. 3701, 3705
- Haykin, S.: *Neural Networks: A Comprehensive Foundation*, 2nd Edn., Prentice-Hall, Englewood Cliffs, NJ, 1999 3701, 3705
- Keppenne, C. L. and Ghil, M.: Adaptive filtering and prediction of the Southern Oscillation index, *J. Geophys. Res.*, 97, 20449–20454, 1992. 3701, 3703
- 20 Keppenne, C. L. and Ghil, M.: Adaptive filtering and prediction of noisy multivariate signals: An application to subannual variability in atmospheric angular momentum, *Intl. J. Bifurcat. Chaos*, 3, 625–634, 1993. 3701, 3703
- Montgomery, D. C., Johnson, L. A., and Gardiner, J. S.: *Forecasting and Time Series Analysis*, McGraw-Hill, New York, 1990. 3701
- 25 Penland, C., Ghil, M., and Weickmann, K. M. : Adaptive filtering and maximum entropy spectra, with application to changes in atmospheric angular momentum, *J. Geophys. Res.*, 96, 22659–22671, 1991. 3701, 3703, 3709
- Plaut, G., Ghil, M., and Vautard, R.: Interannual and interdecadal variability in 335 years of Central England temperatures, *Science*, 268, 710–713, 1995. 3700
- 30 Rumelhart, D. E., Hinton, G. E., and Williams, R. J.: Learning internal representations by error propagation, in: *Parallel Data Processing*, 1, edited by: Rumelhart, D. E. and McClelland, J. L., The M.I.T. Press, Cambridge, MA, 318–362, 1986. 3706

Natural variability and anthropogenic effects in a Central Mediterranean core

S. Alessio et al.

[Title Page](#)[Abstract](#)[Introduction](#)[Conclusions](#)[References](#)[Tables](#)[Figures](#)[⏪](#)[⏩](#)[◀](#)[▶](#)[Back](#)[Close](#)[Full Screen / Esc](#)[Printer-friendly Version](#)[Interactive Discussion](#)

Shackleton, N. J. and Kennet, J. P.: Palaeo-temperature history of the Cenozoic and the initiation of Antarctic glaciation: Oxygen and carbon isotope analysis in DSDP sites 277, 279 and 281, in: Initial Reports of the Deep Sea Drilling Project, edited by: Kennet, J. P. and Houtz, R. E., US Government Printing Office, Washington, DC, USA, 5, 743–755, 1975. 3708

Taricco, C., Alessio, S., and Vivaldo, G.: Sequence of eruptive events in the Vesuvio area recorded in shallow-water Ionian Sea sediments, *Nonlin. Processes Geophys.*, 15, 25–32, doi:10.5194/npg-15-25-2008, 2008. 3701

Taricco, C., Ghil, M., Alessio, S., and Vivaldo, G.: Two millennia of climate variability in the Central Mediterranean, *Clim. Past*, 5, 171–181, doi:10.5194/cp-5-171-2009, 2009. 3700, 3701, 3702, 3708, 3709, 3713

Vautard, R. and Ghil, M.: Singular spectrum analysis in nonlinear dynamics, with applications to paleoclimatic time series, *Physica D*, 35, 395–424, 1989. 3700

Vautard, R., Yiou, P., and Ghil, M.: Singular-spectrum analysis: A toolkit for short, noisy chaotic signals, *Physica D*, 58, 95–126, 1992. 3703

Versteegh, G. J. M., de Leeuw, J. W., Taricco, C., and Romero, A.: Temperature and productivity influences on U_k37 and their possible relation to solar forcing of the Mediterranean winter, *Geochem. Geophys. Geosy.*, 8, Q09005, doi:10.1029/2006GC001543, 2007. 3708

Vivaldo, G., Taricco, C., Alessio, S., and Ghil, M.: Accurate dating of Gallipoli Terrace (Ionian Sea) sediments: Historical eruptions and climate records, *PAGES News*, 17, 8–9, 2009. 3701

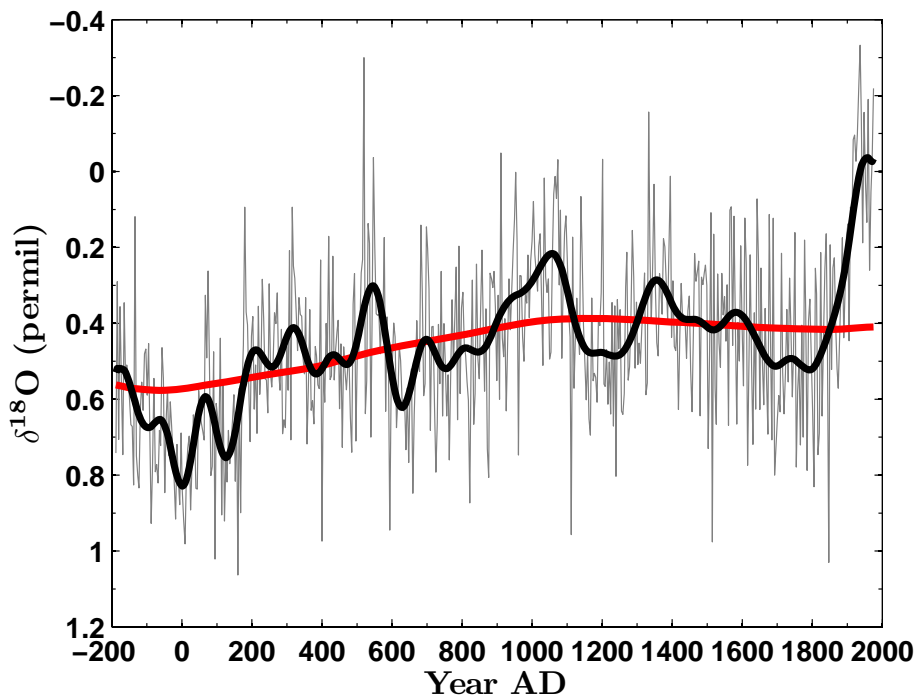


Fig. 1. Time series of $\delta^{18}\text{O}$ from the GT90/3 core and its components. Gray light curve: raw data; black heavy curve: sum of centennial-to-millennial components + $\delta^{18}\text{O}$ mean value; red heavy curve: trend + $\delta^{18}\text{O}$ mean value. The $\delta^{18}\text{O}$ -axis is reversed, here and in subsequent figures, to agree in tendency with temperature. The SSA results plotted here correspond to a window width of ≈ 600 yr; they have been shown to be significant at the 99% level and robust for a wide range of window widths by Taricco et al. (2009).

Natural variability and anthropogenic effects in a Central Mediterranean core

S. Alessio et al.

Title Page

Abstract Introduction

Conclusions References

Tables Figures

⏪ ⏩

◀ ▶

Back Close

Full Screen / Esc

Printer-friendly Version

Interactive Discussion



Natural variability and anthropogenic effects in a Central Mediterranean core

S. Alessio et al.

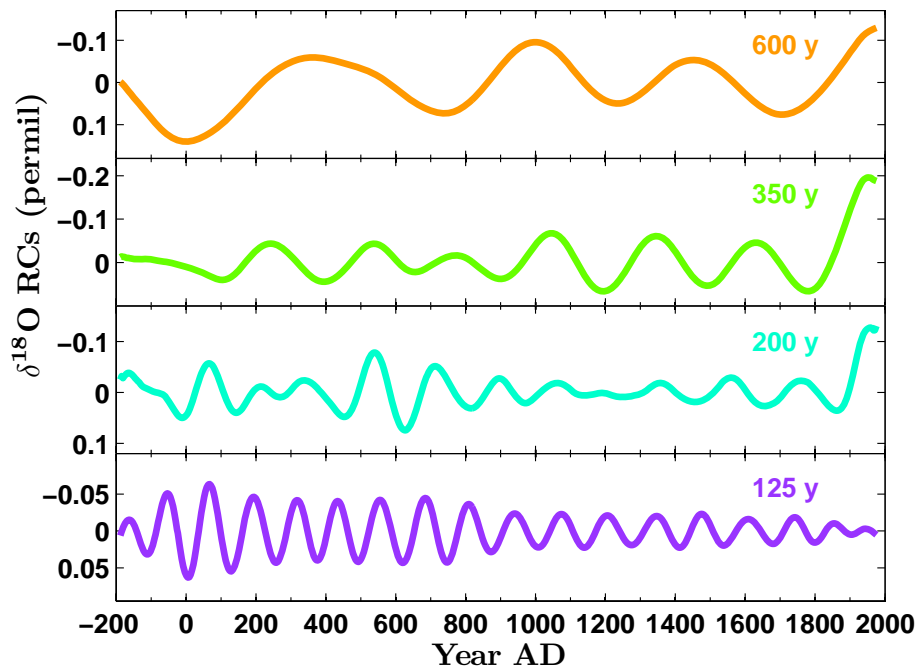


Fig. 2. Significant oscillatory components in the $\delta^{18}\text{O}$ series of core GT90/3, obtained by SSA with a window width of ≈ 600 yr; only the oscillations within the centennial range are plotted here. They correspond to RCs 2–3, 4–5, 6–7–8 and 9–10, respectively.

Natural variability and anthropogenic effects in a Central Mediterranean core

S. Alessio et al.

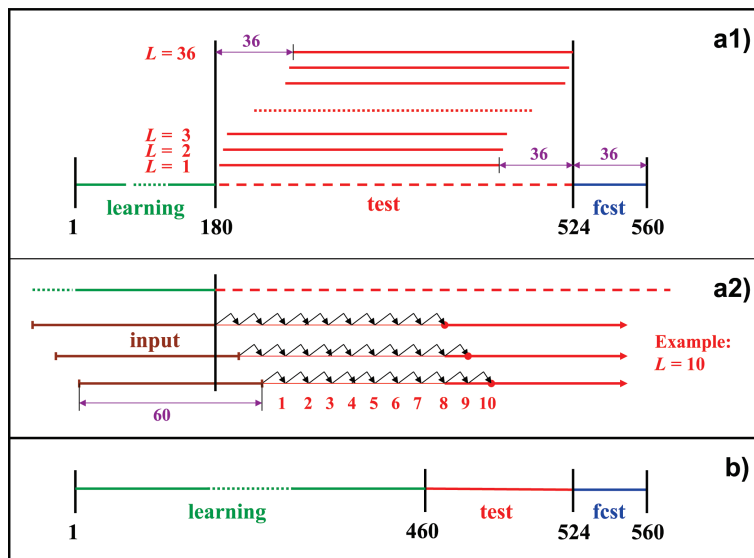


Fig. 3. Schematic diagram of the learning (green), testing (red) and forecasting (blue) sections. The numbers in black indicate the boundaries of the three sections, in number of samples, while the numbers in purple indicate lengths. The length of the forecasting section is $L_{\max} = 36$ samples. **(a1)** Here the learning section has length $N_{\text{learn}} = 180$ samples and the test section has a total length of $N_{\text{test}} = 344$ samples; the tests are carried out over a sliding window whose length K is fixed, $K = 308$ samples, and whose position shifts ahead with increasing lead (red segments). The sliding window provides K pairs of predicted–true values for computing the root-mean-square (rms) forecast errors $R(L)$ at every lead time $\{L: 1 \leq L \leq L_{\max} = 36\}$; see text for details. **(a2)** Example of iterative one-step-into-the-future forecast producing the first three samples of the sliding window in the position that corresponds to lead $L = 10$ samples. Input true samples are represented by brown segments. **(b)** An alternative approach with a longer learning section of $N_{\text{learn}} = 460$ samples, a shorter test section of $N_{\text{test}} = 64$ samples, and no sliding window. In this case, the rms error is evaluated globally over all leads.

Title Page

Abstract Introduction

Conclusions References

Tables Figures

◀ ▶

◀ ▶

Back Close

Full Screen / Esc

Printer-friendly Version

Interactive Discussion



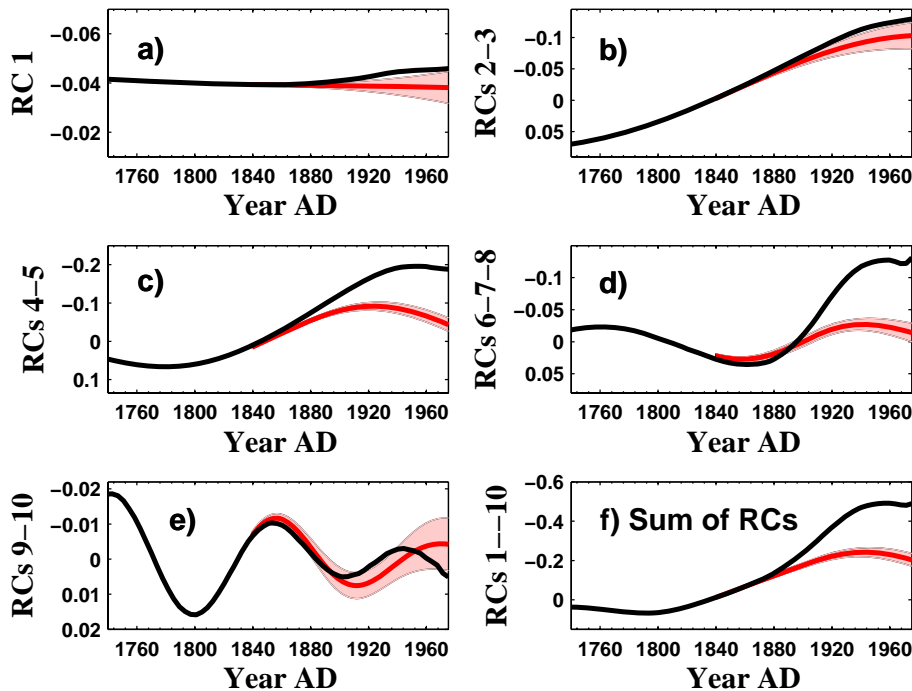


Fig. 4. Prediction results for the $\delta^{18}\text{O}$ time series during the Industrial Era, taken here as 1840–1979 AD; the low-pass filtered observations y_{obs} are shown back to ≈ 1740 AD, to give a better feeling for the range of natural variability. **(a)–(e)** Results for individual narrow-band signals: **(a)** the trend given by RC1; **(b)–(e)** oscillatory signals given by RCs 2–3, 4–5, 6–8 and 9–10, respectively; **(f)** result for the sum of the ten leading RCs, 1–10. Black curves: observed narrow-band signals extracted from the total $\delta^{18}\text{O}$ series; red curves: forecast obtained by the AR approach, accompanied by pink shading giving the forecast uncertainty, based on the performance $R = R(L)$ of the individual narrow-band-signal forecasts over the testing section (see text for details).

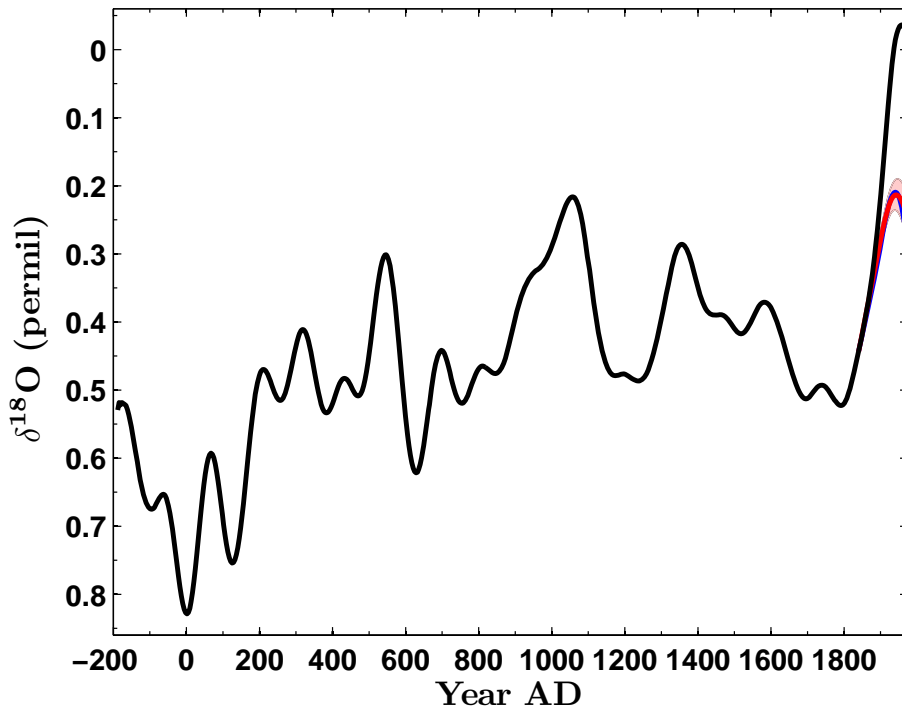


Fig. 5. Total $\delta^{18}\text{O}$ SSA-AR forecast $y_{\text{pred}}(t)$ (red curve) for the Industrial Era and observed values $y_{\text{obs}}(t)$ (black curve) over the entire 2200 y covered by our record. Both $y_{\text{pred}}(t)$ and $y_{\text{obs}}(t)$ represent the climatic LFV recorded in the $\delta^{18}\text{O}$ of core GT90/3, namely the ten leading RCs; for consistency, the mean $\delta^{18}\text{O}$ value has been added back in, see Eq. (1). Pink shading: forecast error of the total SSA-AR forecast, based on the five forecasts of the narrow-band signals, see Fig. 4; and blue curve: sum of the narrow-band-signal forecasts obtained by neural network prediction; see text for details.

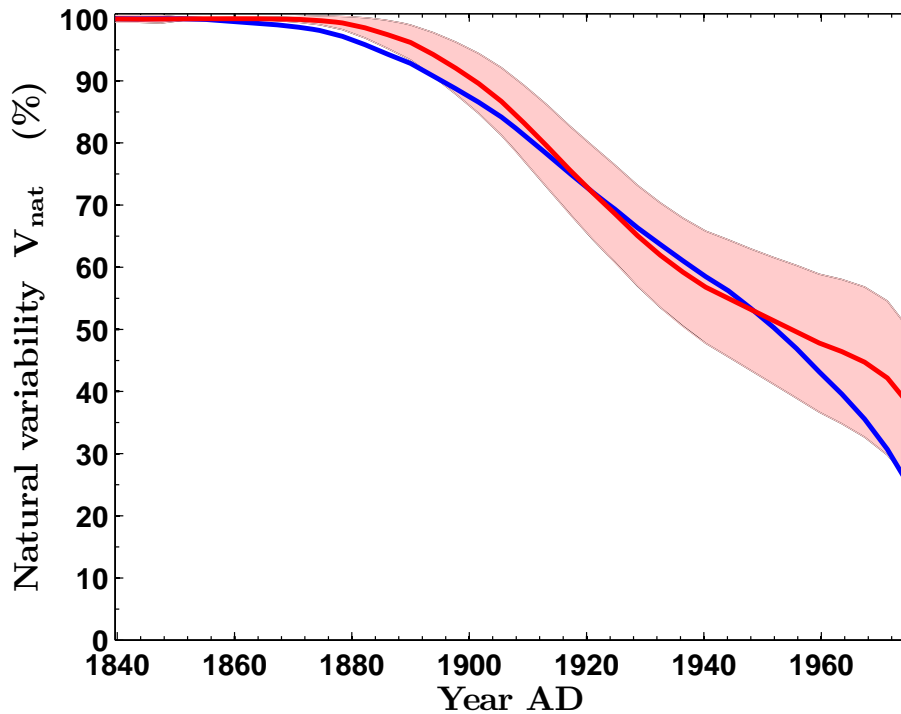


Fig. 6. Fraction $V_{\text{nat}}(t)$ of natural variability in the $\delta^{18}\text{O}$ series for the Industrial Era. Red curve: for the SSA-AR method, with pink shading for the corresponding error belt; and blue curve: for the neural-network prediction. Both are calculated according to Eq. (3) and shown as percentages.

Natural variability and anthropogenic effects in a Central Mediterranean core

S. Alessio et al.

Title Page

Abstract

Introduction

Conclusions

References

Tables

Figures

◀

▶

◀

▶

Back

Close

Full Screen / Esc

Printer-friendly Version

Interactive Discussion

